

Generation of quasi-monoenergetic proton beams via quantum radiative compression

Feng Wan,¹ Wei-Quan Wang,² Qian Zhao,¹ Hao Zhang,² Tong-Pu Yu,^{2,*} Wei-Min Wang,³ Wen-Chao Yan,^{4,5} Yong-Tao Zhao,¹ Karen Z. Hatsagortsyan,⁶ Christoph H. Keitel,⁶ Sergei V. Bulanov,^{7,8} and Jian-Xing Li^{1,†}

¹MOE Key Laboratory for Nonequilibrium Synthesis and Modulation of Condensed Matter, School of Physics, Xi'an Jiaotong University, Xi'an 710049, China

²Department of Physics, National University of Defense Technology, Changsha, 410073, China

³Department of Physics and Beijing Key Laboratory of Opto-electronic Functional Materials and Micro-nano Devices, Renmin University of China, Beijing 100872, China

⁴Key Laboratory for Laser Plasmas (MOE), School of Physics and Astronomy, Shanghai Jiao Tong University, Shanghai, 200240, China

⁵Collaborative Innovation Center of IFSA (CICIFSA), Shanghai Jiao Tong University, Shanghai 200240, China

⁶Max-Planck-Institut für Kernphysik, Saupfercheckweg 1, 69117 Heidelberg, Germany

⁷Institute of Physics ASCR, v.v.i. (FZU), ELI BEAMLINES, Za Radnicí 835, Dolní Břežany, 252241, Czech Republic

⁸Kansai Photon Science Institute, National Institutes for Quantum and Radiological Science and Technology, 8-1-7 Umemidai, Kizugawa-shi, Kyoto, 619-0215, Japan

(Dated: May 25, 2022)

Dense high-energy monoenergetic proton beams are vital for wide applications, thus modern laser-plasma-based ion acceleration methods are aiming to obtain high-energy proton beams with energy spread as low as possible. In this work, we put forward a quantum radiative compression method to post-compress a highly accelerated proton beam and convert it to a dense quasi-monoenergetic one. We find that when the relativistic plasma produced by radiation pressure acceleration collides head-on with an ultraintense laser beam, large-amplitude plasma oscillations are excited due to quantum radiation-reaction and the ponderomotive force, which induce compression of the phase space of protons located in its acceleration phase with negative gradient. Our three-dimensional spin-resolved QED particle-in-cell simulations show that hollow-structure proton beams with a peak energy \sim GeV, relative energy spread of few percents and number $N_p \sim 10^{10}$ (or $N_p \sim 10^9$ with a 1% energy spread) can be produced in near future laser facilities, which may fulfill the requirements of important applications, such as, for radiography of ultra-thick dense materials, or as injectors of hadron colliders.

Laser-plasma-based ion acceleration can provide a much higher acceleration gradient (from GeV/m up to TeV/m), larger beam density (\sim 1% solid density) and shorter beam duration (fs-ps) than conventional electrostatic or radio-frequency accelerators [1, 2]. Benefited from the compactness and low expenses, these ion sources are of paramount significance in broad applications, such as, material tomography [3, 4], plasma radiography [5, 6], cancer therapy [7–9], inertial confinement fusion (ICF) [10–12], and nuclear physics [13]. Generally, they require dense high-energy ion bunches with a rather low energy spread, for instance, the energy spread of hundreds-of-MeV proton beam in the cancer therapy is limited to \lesssim 1% [2], that of hundreds-of-GeV (up to TeV) proton beam in the high precision experiments of high-energy physics is in the order of 10^{-4} [14, 15], and the resolution of proton radiography highly relies on the proton flux, energy and spread [4]. Thus, high-flux high-energy monoenergetic proton beams are in great demand.

Recently, with rapid developments of ultraintense ultrashort laser techniques the peak intensities of modern laser pulses have achieved $I_0 \sim 5 \times 10^{22}$ W/cm² with pulse duration of tens of femtoseconds and energy fluctuation \sim 1% [16–18]. Meanwhile, under-construction or upgrading laser facilities, (e.g. ELI-beamlines [19], SULF [20], Apollon [21], etc.) are

aimed at intensities higher than 10^{23} W/cm². With such intense lasers novel laser-plasma-based ion acceleration schemes attract broad attention. For instance, a hybrid scheme of radiation pressure sheath acceleration is experimentally demonstrated, achieving generation of proton beams with cutoff energy \sim 100 MeV, and with an exponentially rolling off plateau in the spectrum [22]. Collisionless shock acceleration can generate $\sim 10^5$ protons with a peak energy \sim 20 MeV, and energy spread \sim 1% [23] (similarly, about 10^9 protons of 9 MeV with an energy spread \sim 30% are obtained in [24]), while hole-boring radiation pressure acceleration (RPA) at $I_0 \approx 10^{20}$ W/cm² can produce a maximal energy per nucleon \lesssim 30 MeV with energy spread \sim 30% [25–28]. By contrast, light-sail RPA [29], due to the advantages in the energy conversion and scaling, could generate much higher-energy protons (typically \sim GeV; further acceleration to tens of GeV might be influenced and even interrupted because of the Rayleigh-Taylor-like instability) with energy spread of tens of percents in three-dimensional (3D) simulations (those in less realistic two-dimensional (2D) simulations could be narrower) [30–37]. Radiation reaction in the classical regime [38] is shown to improve the quality of RPA beams [39, 40]. As is known, in light-sail RPA to obtain GeV and even higher-energy protons, the energy scaling law requires a high laser intensity of $I_0 \gtrsim 10^{23}$ W/cm². In such an intense laser field though quantum radiation-reaction (QRR) effects [41] will play a significant role in the plasma dynamics and must be taken into account [42–44]. For instance, the proton energy spectra can be essentially disturbed by the

* tongpu@nudt.edu.cn

† jianxing@xjtu.edu.cn

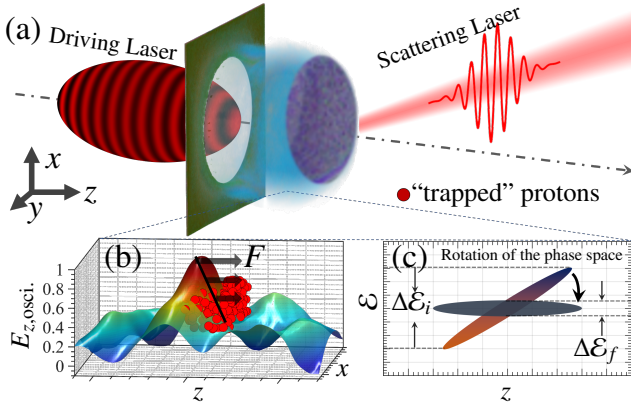


FIG. 1. Interaction scenario. (a): The accelerated plasma via light-sail RPA by an intense CP driving laser collides with another intense LP scattering laser after the completed main acceleration phase. (b): Protons are then “trapped” and further accelerated by the periodic oscillating longitudinal field $E_{z,\text{osci.}}$, induced by QRR effects and the ponderomotive force. The black-solid line and black arrows represent the negative gradient of $E_{z,\text{osci.}}$ and the acceleration force F , respectively. Longer arrows denote larger F . (c): The energy spread of protons is compressed by $E_{z,\text{osci.}}$ due to the rotation of their phase space.

stochastic nature of photon emission [44]. Moreover, recent studies suggest that the electron and photon polarization can reshape QRR and related plasma dynamics [45–47]. Thus, the generation of dense GeV monoenergetic proton beams is still a great challenge.

In this Letter, we put forward a quantum radiative compression (QRC) method to generate dense GeV quasi-monoenergetic proton beams [see the interaction scenario in Fig. 1(a)]. In addition to the common light-sail RPA, when a circularly polarized (CP) laser pulse irradiates an ultra-thin target to generate and accelerate plasma, we apply another intense linearly polarized (LP) laser pulse head-on colliding with the accelerated plasma after RPA stage. In the second stage QRR dominates the plasma dynamics, inducing plasma oscillations with the assistance of the laser ponderomotive force. Consequently, an oscillating longitudinal electric field $E_{z,\text{osci.}}$ inside the plasma is excited and further accelerates and compresses protons to form a dense quasi-monoenergetic proton beam: initially lower-energy protons experience a larger acceleration force of the plasma oscillations F to gain more energy and thus catch up initially higher-energy ones (resulting in a rotation of the phase space) [see Figs. 1(b) and (c) and detailed explanations in Figs. 3 and 4]. We underline that in the QRC process the scattering laser and QRR are indispensable [see Fig. 2]. To describe the plasma dynamics accurately in the applied QRR regime, we have implemented the spin-resolved Monte Carlo processes of electron dynamics and radiation [47–51] into the 3D particle-in-cell (PIC) code EPOCH [52]. With up-coming laser facilities [16–21], proton bunches with a peak energy of GeV order, relative energy spread of few percents and total number $N_p \sim 10^{10}$ can be obtained [see Fig. 2], to the benefit of many applications.

Sample results of generated dense GeV quasi-monoenergetic proton beams are illustrated in Fig. 2. When choosing the

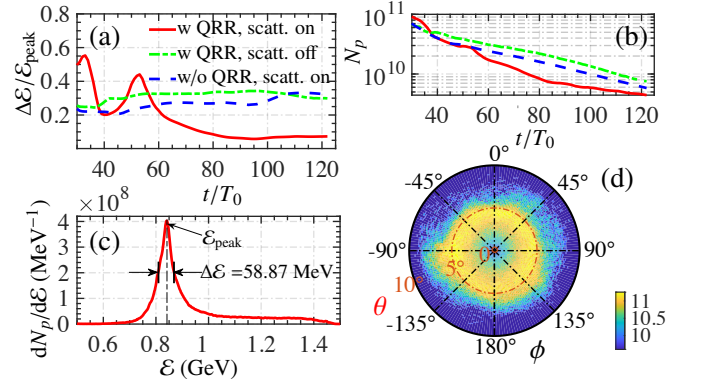


FIG. 2. Generation of quasi-monoenergetic proton beam. (a) and (b): Time evolutions of the relative energy spread $\Delta E/E_{\text{peak}}$ and number N_p of the protons collected from the cylinder with a $7\mu\text{m}$ radius along the propagating axis of the driving laser. ΔE is the absolute energy spread (FWHM) of the density spectrum [see (c)]. The red-solid, green-dash-dotted and blue-dashed curves indicate the cases including the QRR effects and scattering laser, including QRR but no scattering laser, and including scattering laser but no QRR, respectively. Here $t = 0$ is redefined as the time of the driving laser reaching the left boundary of the simulation box (i.e. t_1 given in the text). (c) and (d): For the case including QRR and scattering laser, the energy spectrum $dN_p/dE(\text{MeV}^{-1})$ and corresponding angular distribution $\log_{10}(d^2N_p/d\theta d\phi)$ of collected protons at $t = 98T_0$. θ and ϕ are the polar and azimuthal angles, respectively. Other laser and target parameters are given in the text.

laser and plasma parameters we ensure fulfilling the conditions for the relativistic transparency, light-sail RPA, and for the domination of QRR with respect to the laser ponderomotive force, as given in the following. The peak intensity of the CP driving laser is $I_{d0} \approx 8.56 \times 10^{22} \text{W/cm}^2$ (the corresponding invariant field parameter $a_{d0} = eE_0/m_e c \omega_d \approx \sqrt{\frac{I_{d0}}{1.37 \times 10^{18} \text{W/cm}^2}} \lambda_d [\mu\text{m}] \approx 250$ with wavelength $\lambda_d = 1\mu\text{m}$). $-e$ and m_e are the charge and mass of electron, respectively, E_0 and ω_d the amplitude and frequency of the driving laser, respectively, and c the light speed in vacuum. The profile of the driving laser pulse is $\frac{1}{2} \exp\left(-\frac{r^4}{w_{d0}^4}\right) \{\tanh[2(t-t_1)] - \tanh[2(t-t_2)]\}$, with coordinate $r = \sqrt{x^2 + y^2}$ and focal radius $w_{d0} = 6\mu\text{m}$. $t_1 = 88T_0$ and $t_2 = 98T_0$ are the times of the front and tail of the driving laser entering the simulation box, respectively, with laser period T_0 , and the pulse duration $\tau_d = t_2 - t_1$. We consider a fully ionized polystyrene target composed of e^- , C^{6+} and H^+ , with number densities $n_e(e^-) = 300n_c$ and $n_p(H^+) = n_c(C^{6+}) = n_e(e^-)/7$, and target thickness $l = 0.3\mu\text{m}$. $n_c = m_e \omega_d^2 / 4\pi e^2$ is the critical plasma density. The laser and target parameters are optimized to meet the partially relativistic transparency condition $l/\lambda_d \approx a_{d0} n_c / \pi n_e \approx 0.3$ [53, 54], which can suppress the target-deformation-induced instability [55]. For the LP scattering laser, the peak intensity is $I_{s0} \approx 8.56 \times 10^{22} \text{W/cm}^2$ ($a_{s0} = 250$) with wavelength $\lambda_s = \lambda_d$, and the profile $\frac{1}{2} \exp\left(-\frac{r^2}{w_{s0}^2}\right) \{\tanh[2(t-t_3)] - \tanh[2(t-t_4)]\}$ with focal radius $w_{s0} = 7\mu\text{m}$. $t_3 = 3T_0$ and $t_4 = 19T_0$ are the times of the front and tail of the scattering laser enter-

ing the simulation box, respectively, and the pulse duration $\tau_s = t_4 - t_3$. These synchronized two laser beams will be feasible soon by employing those multi-beam petawatt facilities or by splitting one laser beam in multi-petawatt laser facilities (e.g., ELI-Beamlines, SULF and Apollon [16–21]). The 3D simulation box is placed at $-20\mu\text{m} \leq z \leq 100\mu\text{m}$, $-15\mu\text{m} \leq x \leq 15\mu\text{m}$ and $-15\mu\text{m} \leq y \leq 15\mu\text{m}$, with mesh size $n_z \times n_x \times n_y = 6000 \times 300 \times 300$. The target is placed at $-18.65\mu\text{m} \leq z \leq -18.35\mu\text{m}$ and represented by 150 macro-electrons, 50 macro-protons and 10 macro-carbon ions per cell. In the following, the electromagnetic fields E and B are normalized by $e/m_e c \omega_s$, the number density n by n_c , and the charge density ρ by $n_c e$.

For the given parameters, during light-sail RPA the electrons can be accelerated up to about 50 MeV with relativistic Lorentz factor $\gamma_e \approx 100$; see [56]. Afterwards, they head-on collide with the scattering laser to emit photons via nonlinear Compton scattering. The strong field quantum parameter in this setup is $\chi_e = (\hbar\omega_s/m_e c^2)\gamma_e a_{s0}[1 - v_e \cos(\theta_{\text{coll}})]/c \sim 0.01 - 0.1$, which indicates that the QRR effects are not negligible [41], however, further electron-positron pair production via nonlinear Breit-Wheeler process is suppressed [41, 57]. Here v_e is the electron velocity and θ_{coll} the collision angle. Our analysis in Figs. 3 and 4 shows that indeed the electron motion is affected by QRR, and what is more remarkable, it has significant consequences for the ion dynamics due to the modification of charge separation forces. Time evolutions of the relative energy spread $\Delta\mathcal{E}/\mathcal{E}_{\text{peak}}$ and number N_p of collected protons along the propagation axis of the driving laser are shown in Figs. 2(a) and (b). As including the scattering laser and QRR effects, before $t \approx 33T_0$ the relative energy spread $\Delta\mathcal{E}/\mathcal{E}_{\text{peak}}$ first increases since the scattering laser pushes the electrons and consequently increases $\Delta\mathcal{E}$ by charge separation forces; in the range of $33T_0 \lesssim t \lesssim 53T_0$ instead $\Delta\mathcal{E}/\mathcal{E}_{\text{peak}}$ is unstable because even though the scattering laser has left the protons are not stably phase-matched with the excited oscillating longitudinal field $E_{z,\text{osci}}$. (see [56]); after $t \approx 53T_0$ the $E_{z,\text{osci}}$ is becoming stable, and the protons are gradually phase-matched with $E_{z,\text{osci}}$ and substantially compressed by $E_{z,\text{osci}}$ (negative gradient) from initial $\Delta\mathcal{E}/\mathcal{E}_{\text{peak}} \geq 40\%$ down to $\Delta\mathcal{E}/\mathcal{E}_{\text{peak}} \lesssim 6\%$, which keeps stable as $t \geq 80T_0$ [see scenario in Figs. 1(b) and (c) and physical reasons in Figs. 3 and 4]. The proton number N_p is continuously reduced due to the transverse momenta. On the contrary, as excluding the scattering laser (common setup) or artificially removing the QRR effects (in which electron dynamics is governed by the Lorentz force only, and the electron spin by the Thomas-Bargmann-Michel-Telegdi equation [58–60]), $\Delta\mathcal{E}/\mathcal{E}_{\text{peak}}$ is always large ($\sim 25\% - 35\%$). Thus, QRR effects and the ponderomotive force, both provided by the scattering laser, result in the generation of a quasi-monoenergetic proton beam; see the specific energy spectrum and angular distribution in Figs. 2(c) and (d). The final peak energy is $\mathcal{E}_{\text{peak}} \approx 839\text{MeV}$ with $\Delta\mathcal{E}/\mathcal{E}_{\text{peak}} \approx 6\%$, total number $N_p \approx 4.6 \times 10^9$, and radial angular divergence $\theta \approx 68\text{mrad}$ (about 3.9°). And, $N_p \approx 10^9$ within 1% energy spread at $\mathcal{E}_{\text{peak}}$ can be obtained. Such a proton beam may serve as an injector for a hadron collider or ion radiography source for ultra-thick targets [2, 61]. Moreover, the proton beam has a

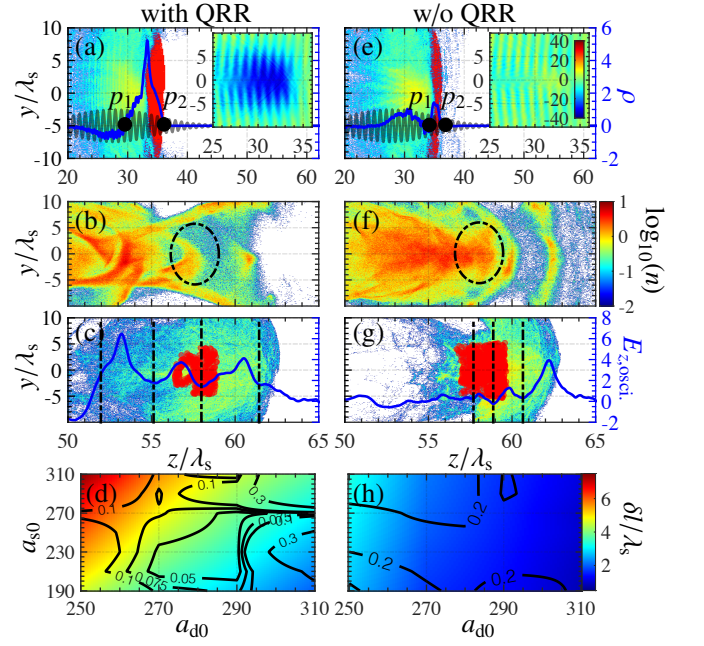


FIG. 3. (a) and (e): Number density distributions of ions ($6n_c + n_p$, red) and electrons (n_e , colored background) at $t = 66T_0$. Note that to show the relative slippage between electrons and ions, here ions are partially shaded by electrons. Solid-gray and solid-blue curves indicate normalized scattering laser profile and charge density ρ on the propagation axis ($y = 0$), respectively. Black dots p_1 and p_2 denote $\rho(p_1) = \rho(p_2) = 0$, and the relative slippage distance between the electron and ion layer is defined as $\delta l \equiv z(p_2) - z(p_1)$. Subfigures with color bar show the corresponding dimensionless longitudinal electric field E_z . The corresponding electron energy spectrum is given in [56]. (b) and (f): Number density of electrons n_e at $t = 94T_0$. Black-dashed circles denote the positions of traced protons [shown in red in (c) and (g)]. (c) and (g): Number density of protons n_p at $t = 94T_0$. Traced protons in FWHM of the proton energy spectra [i.e. $\Delta\mathcal{E}$; see Fig. 2(c)] are labeled in red. Solid-blue curves denote $E_{z,\text{osci}}$ on the propagation axis ($y = 0$), and the black-dashed curves are used to distinguish different field cycles. (b)-(c) and (f)-(g) share the same color bar. In (a)-(c) and (e)-(g) $a_{s0} = 300$. (d) and (h): Correlation between δl (hot map) and $\Delta\mathcal{E}/\mathcal{E}_{\text{peak}}$ (contour) with respect to a_{d0} and a_{s0} . Left and right columns show the cases including and excluding the QRR effects, respectively, and the scattering laser is always included. Here 2D simulations are employed for simplicity. Other parameters are the same as those in Fig. 2.

hollow structure [see Fig. 2(d)] which may find an application as a high-energy positron collimator [62]. Note that here the impact of spin effects on the proton dynamics is insignificant, in contrast to Refs. [47, 50, 57], since the employed target is not initially spin-polarized and the pair production is negligible.

The physics behind the proton QRC process is analyzed in Figs. 3 and 4. Due to the relativistic-transparency effects and Rayleigh-Taylor like instability, the driving laser will penetrate through the electron layer and induce an energy spread of accelerated protons [30]. Higher-energy protons move faster, and consequently, the target continues to expand [29, 30]. When the scattering laser head-on collides with the plasma, the electrons are decelerated by the scattering laser and left behind

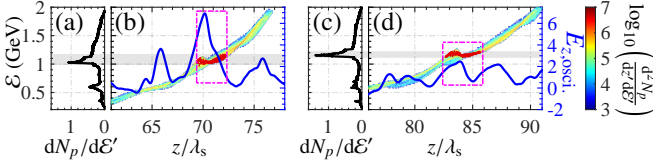


FIG. 4. Simulations with QRR and scattering laser. (a) and (c): Energy spectra dN_p/dE' normalized by a factor of 9.39×10^{16} vs E' at $t = 114T_0$ and $t = 130T_0$, respectively. $E' \equiv E'/\text{GeV}$. (b) and (d): $\log_{10}(\frac{d^2 N_p}{dz' dE'})$ with respect to $z' = z/\lambda_s$ and E' at $t = 114T_0$ and $t = 130T_0$, respectively. The blue lines and red particles indicate $E_{z,\text{osci.}}(y = 0)$ and traced protons, respectively. The gray bands in (a)-(d) denote ΔE . Other parameters are the same as those in Fig. 3.

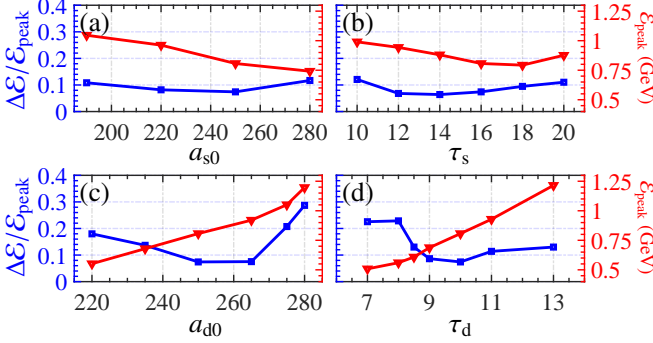


FIG. 5. (a)-(d) Impact of a_{s0} , τ_s , a_{d0} and τ_d on $\mathcal{E}_{\text{peak}}$ and $\Delta\mathcal{E}/\mathcal{E}_{\text{peak}}$, respectively. Other parameters are the same as those in Fig. 2.

the protons with a slippage distance δl , and the corresponding charge separation between electrons and protons along with the current flow can excite a strong longitudinal electric field $E_z = E_{z,\text{stat.}} + E_{z,\text{curr.}} < 0$ [see Fig. 3(a)]. Here the current-flow-induced $E_{z,\text{curr.}} > 0$ is mainly derived from those protons moving faster than electrons, and $E_{z,\text{curr.}}$ reduces $|E_z|$ (the charge separation field $E_{z,\text{stat.}} < 0$). When the scattering laser left, the electrons will be re-accelerated by $E_z < 0$ and excite a plasma oscillation $E_{z,\text{osci.}}$ [see Figs. 3(b) and (c)]. The protons synchronized with its negative-gradient phase ($E_{z,\text{osci.}} > 0, \partial_z E_{z,\text{osci.}} < 0$) can be “trapped” and experience an energy-dependent acceleration field [see Fig. 3(c) and the scenario in Figs. 1(b) and (c)]. For instance, the protons locating near $z \approx 56.6\lambda_s$ are subjected to $E_{z,\text{osci.}} \approx 4.0$, which is stronger than $E_{z,\text{osci.}} \approx 1.7$ near $z \approx 58\lambda_s$. Since the proton energy is approximately linearly proportional to its longitudinal position (i.e., lower-energy protons move relatively slower than higher-energy ones and thus are at the rear), $E_{z,\text{osci.}}$ with negative-gradient can provide stronger acceleration for lower-energy protons near $z \approx 56.6\lambda_s$. Consequently, the protons can be compressed in energy space to yield a low-energy-spread bunch [see Figs. 2 and 4].

Note that the compression efficiency is determined by the amplitude of $E_{z,\text{osci.}}$ and its spatial gradient $\partial_z E_{z,\text{osci.}}$, which both rely on E_z , and the oscillation wavelength is $\lambda_{\text{osci.}} \sim \delta l$. Since $E_z = E_{z,\text{stat.}} + E_{z,\text{curr.}}$ and $E_{z,\text{stat.}}$ is also proportional to δl , thus δl plays a key role in the excitation of $E_{z,\text{osci.}}$, and it is induced by the ponderomotive force F_p and QRR force

F_{QRR} [56, 63]. Here, the relativistic ponderomotive force in z direction is given by $F_{p,z} \approx -\frac{2}{\pi}(1 + c/v_z)\partial_\eta a_s$ [56, 64, 65], where $a_s(\eta)$ is instantaneous invariant field parameter of the scattering laser with laser phase $\eta = k_s z - \omega_s t$, and wave vector $k_s = 2\pi/\lambda_s$. For given parameters, $\max(F_{p,z}) \approx \frac{4a_{s0}}{\pi r_s} \sqrt{\frac{2}{e'}} = 4.4$, where e' is the natural logarithm base. While, the QRR force can be estimated via $F_{\text{QRR}} \approx -\frac{2}{3}\chi_e^2 \alpha_f^2 \frac{\lambda_s}{r_e} g(\chi_e)$ [66–68], where $g(\chi_e) \approx (1 + 8.93\chi_e + 2.41\chi_e^2)^{-2/3}$ is the quantum suppression function, α_f the fine structure constant and r_e the classical electron radius. By averaging over a scattering laser period, $\langle F_{\text{QRR}} \rangle \approx -\frac{4}{3\pi}\chi_e^2 \alpha_f^2 \frac{\lambda_s}{r_e} g(\chi_e')$, where $\chi_e' \approx \frac{2\hbar\omega_s \gamma_e a_{s0}}{m_e c^2} \exp\left(-\frac{\eta^2}{\tau_s^2}\right)$. For $\langle \gamma_e \rangle \approx 70$, $\max\{\langle F_{\text{QRR}} \rangle\} \approx 27$, which is much larger than $\max(F_{p,z})$. Those two forces are balanced by the excited longitudinal field: $|E_z| = |E_{z,\text{curr.}} + E_{z,\text{stat.}}| \approx |F_{p,z} + F_{\text{QRR}}|$. From the simulation results [see E_z in Fig. 3(a)] $\max(|E_z|) \approx 40$ is very close to the estimated $\max(|F_{p,z} + F_{\text{QRR}}|) \approx 32$. We have also estimated $\max(E_{z,\text{stat.}}) = E_{z,\text{stat.}}(p_1) = -\int_{z(p_2)}^{z(p_1)} \rho(z) dz \approx \frac{\rho_{\text{max}} \delta l}{2} \approx -20\pi$ with $\rho_{\text{max}} \approx 4$ and $\delta l \approx 5\lambda_s$, which is in fact larger than $|E_z|$ due to counteracting $E_{z,\text{curr.}} > 0$. The QRC is caused by the further excited oscillation field $E_{z,\text{osci.}} \approx 4 - 5$ with $\lambda_{\text{osci.}} \approx 3\lambda_s$ [see Fig. 3(c)]. The phase space of those “trapped” protons continuously rotates [see Figs. 4(b) and (d)], and the energy spread is reduced approximately from 200 MeV at $t = 114T_0$ to 100 MeV at $t = 130T_0$ [see Figs. 4(a) and (c)]. This compression effects can sustain about 10-30 periods, and the final energy spread can be compressed down to few percents. The correlation between the final energy spread $\Delta\mathcal{E}/\mathcal{E}_{\text{peak}}$ and the slippage δl is illustrated in Fig. 3(d).

As given in the applied condition $F_{\text{QRR}} \gg F_{p,z}$, the key role of QRR for the QRC process is clear, which is described by the QRC parameter $|F_{\text{QRR}}/F_{p,z}| \sim \mathcal{R} \equiv (\chi_e^2 \lambda_s \tau_s / a_{s0}) (\alpha^2 / r_e)$. In fact, as we artificially remove QRR, the compression effects will be greatly suppressed [see Figs. 3(e)-(h)]. In this case $E_{z,\text{peak}} \approx \max(F_{p,z}) \approx 5$ and $\delta l \approx 3\lambda_s$ [see Fig. 3(e)]. $E_{z,\text{osci.}} \approx 1.0$ with $\lambda_{\text{osci.}} \approx \lambda_s$ [see Fig. 3(g)]. And the final compression effects are rather weak [see the correlation between $\Delta\mathcal{E}/\mathcal{E}_{\text{peak}}$ and δl in Fig. 3(h)].

For the experimental feasibility, we investigate the impact of the driving and scattering laser parameters on the QRC efficiency, as shown in Fig. 5. As $190 \leq a_{s0} \leq 280$, $\max(\chi_e) \approx 0.05 \sim 0.07$ and $F_{\text{QRR}} \approx 26.8 - 33.1$, which is still much larger than $F_{p,z}$, and QRC takes place. While at smaller a_{s0} the QRC is suppressed, at larger a_{s0} the QRC will be enhanced up to the point when δl is comparable to the longitudinal thickness of the plasma. In deep quantum regime with $\chi_e (\propto a_{s0}) \gg 1$, the quantum stochasticity also will increase the energy spread of the electrons and further that of the protons [69]. From the parameter \mathcal{R} we can deduce that τ_s plays a similar role as a_{s0} [see Figs. 5(a) and (b)]. Moreover, the driving laser determines the energies of electrons and protons in light-sail RPA and therefore affects many parameters, e.g., χ_e , n_e and n_i . Our 3D simulations show that to obtain $\Delta\mathcal{E}/\mathcal{E}_{\text{peak}} \lesssim 10\%$, the optimal driving laser intensity is $240 \leq a_{d0} \leq 270$ and the pulse duration is $8.5 \leq \tau_d \leq 13$ [see Figs. 5(c) and (d)]. As expected, $\mathcal{E}_{\text{peak}}$ is proportional to a_{d0} and τ_d . However, when a_{d0} is much

lower than the transparency condition, i.e., $a_{d0} \ll \frac{\pi n_e l}{n_c \lambda_d}$ [70, 71], γ_e and χ_e will be much smaller, and consequently F_{QRR} is rather weak and the QRC will be ineffective. On the contrary, if a_{d0} is too high, the target deformation will be much earlier, which will also limit the effective acceleration. τ_d has similar effects: a too short driving laser can not effectively accelerate plasma [e.g. $\tau_d \lesssim 9T_0$ in Fig. 5(d)], while a too long driving laser will generate very high-energy protons, which are hard to be compressed due to limited $E_{z,\text{osci.}}$ and $\lambda_{\text{osci.}}$. Note that these results are collected at $t = 130T_0$, and for longer pulses the energy spectra may be further compressed when extending the simulation sizes.

In conclusion, we have proposed the QRC method to generate dense GeV quasi-monoenergetic proton beams, which is based on QRR effects for the proton dynamics in plasma. With up-coming laser facilities, such as ELI-beamlines, SULF,

Appolon, our 3D spin-resolved QED-PIC simulations show that hollow-structure proton beams with peak energy $\mathcal{E}_{\text{peak}} \sim \text{GeV}$, energy spread $\lesssim 6\%$ and number $N_p \sim 10^{10}$ ($N_p \sim 10^9$ within $\Delta\mathcal{E}/\mathcal{E}_{\text{peak}} \leq 1\%$) can be obtained, which may fulfill the requirements of high-resolution proton imaging, high-energy particle physics and relativistic positron collimation.

Acknowledgment: This work is supported by the National Key Research and Development Program of China (Grant Nos. 2018YFA0404801, 2018YFA0404802), the National Natural Science Foundation of China (Grant Nos. 11875319, 12022506, 12005298, 11874295, 11804269, U1532263), and the Research Project of NUDT (ZK18-02-02; ZK19-25). The work is also supported by the project High Field Initiative (CZ.02.1.01/0.0/0.0/15_003/0000449) from the European Regional Development Fund.

-
- [1] Gerard A. Mourou, Toshiki Tajima, and Sergei V. Bulanov, “Optics in the relativistic regime,” *Rev. Mod. Phys.* **78**, 309–371 (2006).
- [2] Andrea Macchi, Marco Borghesi, and Matteo Passoni, “Ion acceleration by superintense laser-plasma interaction,” *Rev. Mod. Phys.* **85**, 751–793 (2013).
- [3] M. Roth, A. Blazevic, M. Geissel, T. Schlegel, T. E. Cowan, M. Allen, J.-C. Gauthier, P. Audebert, J. Fuchs, J. Meyer ter Vehn, M. Hegelich, S. Karsch, and A. Pukhov, “Energetic ions generated by laser pulses: A detailed study on target properties,” *Phys. Rev. ST Accel. Beams* **5**, 061301 (2002).
- [4] M. Borghesi, A. J. Mackinnon, D. H. Campbell, D. G. Hicks, S. Kar, P. K. Patel, D. Price, L. Romagnani, A. Schiavi, and O. Willi, “Multi-MeV proton source investigations in ultraintense laser-foil interactions,” *Phys. Rev. Lett.* **92**, 055003 (2004).
- [5] M. Borghesi, D. H. Campbell, A. Schiavi, M. G. Haines, O. Willi, A. J. MacKinnon, P. Patel, L. A. Gizzi, M. Galimberti, R. J. Clarke, F. Pegoraro, H. Ruhl, and S. Bulanov, “Electric field detection in laser-plasma interaction experiments via the proton imaging technique,” *Phys. Plasmas* **9**, 2214–2220 (2002).
- [6] A. J. Mackinnon, P. K. Patel, M. Borghesi, R. C. Clarke, R. R. Freeman, H. Habara, S. P. Hatchett, D. Hey, D. G. Hicks, S. Kar, M. H. Key, J. A. King, K. Lancaster, D. Neely, A. Nikkro, P. A. Norreys, M. M. Notley, T. W. Phillips, L. Romagnani, R. A. Snavely, R. B. Stephens, and R. P. J. Town, “Proton radiography of a laser-driven implosion,” *Phys. Rev. Lett.* **97**, 045001 (2006).
- [7] S. V. Bulanov and V. S. Khoroshkov, “Feasibility of using laser ion accelerators in proton therapy,” *Plasma Phys. Rep.* **28**, 453 (2002).
- [8] Dieter Schardt, Thilo Elsässer, and Daniela Schulz-Ertner, “Heavy-ion tumor therapy: Physical and radiobiological benefits,” *Rev. Mod. Phys.* **82**, 383–425 (2010).
- [9] S. V. Bulanov, J. J. Wilkens, M. Molls, T. Zh. Esirkepov, G. Korn, G. Kraft, S. D. Kraft, and V. S. Khoroshkov, “Laser ion acceleration for hadron therapy,” *Physics Uspekhi* **57**, 1149 (2014).
- [10] M. Roth, T. E. Cowan, M. H. Key, S. P. Hatchett, C. Brown, W. Fountain, J. Johnson, D. M. Pennington, R. A. Snavely, S. C. Wilks, K. Yasuike, H. Ruhl, F. Pegoraro, S. V. Bulanov, E. M. Campbell, M. D. Perry, and H. Powell, “Fast ignition by intense laser-accelerated proton beams,” *Phys. Rev. Lett.* **86**, 436–439 (2001).
- [11] N. Naumova, T. Schlegel, V. T. Tikhonchuk, C. Labaune, I. V. Sokolov, and G. Mourou, “Hole boring in a DT pellet and fast-ion ignition with ultraintense laser pulses,” *Phys. Rev. Lett.* **102**, 025002 (2009).
- [12] V.T. Tikhonchuk, T. Schlegel, C. Regan, M. Temporal, J.-L. Feugeas, Ph. Nicolai, and X. Ribeyre, “Fast ion ignition with ultra-intense laser pulses,” *Nucl. Fusion* **50**, 045003 (2010).
- [13] A Macchi, A Sgattoni, S Sinigardi, M Borghesi, and M Passoni, “Advanced strategies for ion acceleration using high-power lasers,” *Plasma Phys. Control. Fusion* **55**, 124020 (2013).
- [14] “CERN, Large Hadron Colliders (LHC), <https://home.cern/science/accelerators/large-hadron-collider/>,”
- [15] “RHIC (Relativistic Heavy Ion Colliders), <https://www.bnl.gov/rhic/>,”
- [16] Jin Woo Yoon, Cheonha Jeon, Junghoon Shin, Seong Ku Lee, Hwang Woon Lee, Il Woo Choi, Hyung Taek Kim, Jae Hee Sung, and Chang Hee Nam, “Achieving the laser intensity of $5.5 \times 10^{22} \text{W/cm}^2$ with a wavefront-corrected multi-PW laser,” *Opt. Express* **27**, 20412 (2019).
- [17] Colin N. Danson, Constantin Haefner, Jake Bromage, Thomas Butcher, Jean-Christophe F. Chanteloup, Enam A. Chowdhury, Almantas Galvanauskas, Leonida A. Gizzi, Joachim Hein, David I. Hillier, Nicholas W. Hopps, Yoshiaki Kato, Efim A. Khazanov, Ryosuke Kodama, Georg Korn, Ruxin Li, Yutong Li, Jens Limpert, Jingui Ma, Chang Hee Nam, David Neely, Dimitrios Papadopoulos, Rory R. Penman, Liejia Qian, Jorge J. Rocca, Andrey A. Shaykin, Craig W. Siders, Christopher Spindloe, Sándor Szatmári, Raoul M. G. M. Trines, Jianqiang Zhu, Ping Zhu, and Jonathan D. Zuegel, “Petawatt and exawatt class lasers worldwide,” *High Power Laser Sci. Eng.* **7**, e54 (2019).
- [18] S Gales, K A Tanaka, D L Balabanski, F Negoita, D Stutman, O Tesileanu, C A Ur, D Ursescu, I Andrei, S Ataman, M O Cernaianu, L D’Alessi, I Dancus, B Diaconescu, N Djourelou, D Filipescu, P Ghenuche, D G Ghita, C Matei, K Seto, M Zeng, and N V Zamfir, “The extreme light infrastructure—nuclear physics (ELI-NP) facility: new horizons in physics with 10 PW ultra-intense lasers and 20 MeV brilliant gamma beams,” *Rep. Progr. Phys.* **81**, 094301 (2018).
- [19] “The Extreme Light Infrastructure (ELI),” <http://www.elibeams.eu/en/facility/lasers/>.
- [20] Ru Xin Li, “Progress of the SULF 10 PW laser project,” in *1st AAPPS-DPP Meeting*.

- [21] “Apollon multi-PW laser Users Facility,” <http://www.polytechnique.edu>.
- [22] A. Higginson, R. J. Gray, M. King, R. J. Dance, S. D. R. Williamson, N. M. H. Butler, R. Wilson, R. Capdessus, C. Armstrong, J. S. Green, S. J. Hawkes, P. Martin, W. Q. Wei, S. R. Mirfayzi, X. H. Yuan, S. Kar, M. Borghesi, R. J. Clarke, D. Neely, and P. McKenna, “Near-100 MeV protons via a laser-driven transparency-enhanced hybrid acceleration scheme,” *Nat. Commun.* **9**, 724 (2018).
- [23] Dan Haberberger, Sergei Tochitsky, Frederico Fiuza, Chao Gong, Ricardo A. Fonseca, Luis O. Silva, Warren B. Mori, and Chan Joshi, “Collisionless shocks in laser-produced plasma generate monoenergetic high-energy proton beams,” *Nat. Phys.* **8**, 95–99 (2011).
- [24] H. Zhang, B. F. Shen, W. P. Wang, S. H. Zhai, S. S. Li, X. M. Lu, J. F. Li, R. J. Xu, X. L. Wang, X. Y. Liang, Y. X. Leng, R. X. Li, and Z. Z. Xu, “Collisionless shock acceleration of high-flux quasimonoenergetic proton beams driven by circularly polarized laser pulses,” *Phys. Rev. Lett.* **119**, 164801 (2017).
- [25] A. Henig, S. Steinke, M. Schnürer, T. Sokollik, R. Hörlein, D. Kiefer, D. Jung, J. Schreiber, B. M. Hegelich, X. Q. Yan, J. Meyer ter Vehn, T. Tajima, P. V. Nickles, W. Sandner, and D. Habs, “Radiation-pressure acceleration of ion beams driven by circularly polarized laser pulses,” *Phys. Rev. Lett.* **103**, 245003 (2009).
- [26] S. Kar, K. F. Kakolee, B. Qiao, A. Macchi, M. Cerchez, D. Doria, M. Geissler, P. McKenna, D. Neely, J. Osterholz, R. Prasad, K. Quinn, B. Ramakrishna, G. Sarri, O. Willi, X. Y. Yuan, M. Zepf, and M. Borghesi, “Ion acceleration in multispecies targets driven by intense laser radiation pressure,” *Phys. Rev. Lett.* **109**, 185006 (2012).
- [27] J. H. Bin, W. J. Ma, H. Y. Wang, M. J. V. Streeter, C. Kreuzer, D. Kiefer, M. Yeung, S. Cousens, P. S. Foster, B. Dromey, X. Q. Yan, R. Ramis, J. Meyer ter Vehn, M. Zepf, and J. Schreiber, “Ion acceleration using relativistic pulse shaping in near-critical-density plasmas,” *Phys. Rev. Lett.* **115**, 064801 (2015).
- [28] C. Scullion, D. Doria, L. Romagnani, A. Sgattoni, K. Naughton, D. R. Symes, P. McKenna, A. Macchi, M. Zepf, S. Kar, and M. Borghesi, “Polarization dependence of bulk ion acceleration from ultrathin foils irradiated by high-intensity ultrashort laser pulses,” *Phys. Rev. Lett.* **119**, 054801 (2017).
- [29] T. Esirkepov, M. Borghesi, S. V. Bulanov, G. Mourou, and T. Tajima, “Highly efficient relativistic-ion generation in the laser-piston regime,” *Phys. Rev. Lett.* **92**, 175003 (2004).
- [30] F. Pegoraro and S. V. Bulanov, “Photon bubbles and ion acceleration in a plasma dominated by the radiation pressure of an electromagnetic pulse,” *Phys. Rev. Lett.* **99**, 065002 (2007).
- [31] Andrea Macchi, Federica Cattani, Tatiana V. Liseykina, and Fulvio Cornolti, “Laser acceleration of ion bunches at the front surface of overdense plasmas,” *Phys. Rev. Lett.* **94**, 165003 (2005).
- [32] M. Chen, A. Pukhov, T. P. Yu, and Z. M. Sheng, “Enhanced collimated GeV monoenergetic ion acceleration from a shaped foil target irradiated by a circularly polarized laser pulse,” *Phys. Rev. Lett.* **103**, 024801 (2009).
- [33] Tong-Pu Yu, Alexander Pukhov, Gennady Shvets, and Min Chen, “Stable laser-driven proton beam acceleration from a two-ion-species ultrathin foil,” *Phys. Rev. Lett.* **105**, 065002 (2010).
- [34] S. V. Bulanov, E. Yu. Echkina, T. Zh. Esirkepov, I. N. Inovenkov, M. Kando, F. Pegoraro, and G. Korn, “Unlimited ion acceleration by radiation pressure,” *Phys. Rev. Lett.* **104**, 135003 (2010).
- [35] Liangliang Ji, Alexander Pukhov, and Baifei Shen, “Ion acceleration in the ‘dragging field’ of a light-pressure-driven piston,” *New J. Phys.* **16**, 063047 (2014).
- [36] M. L. Zhou, X. Q. Yan, G. Mourou, J. A. Wheeler, J. H. Bin, J. Schreiber, and T. Tajima, “Proton acceleration by single-cycle laser pulses offers a novel monoenergetic and stable operating regime,” *Phys. Plasmas* **23**, 043112 (2016).
- [37] Y. Wan, I. A. Andriyash, C. H. Pai, J. F. Hua, C. J. Zhang, F. Li, Y. P. Wu, Z. Nie, W. B. Mori, W. Lu, V. Malka, and C. Joshi, “Ion acceleration with an ultra-intense two-frequency laser tweezer,” *New J. Phys.* **22**, 052002 (2020).
- [38] L. D. Landau and E. M. Lifshitz, *The Classical Theory of Fields* (Elsevier, Oxford, 1975).
- [39] M. Tamburini, F. Pegoraro, A. Di Piazza, C. H. Keitel, and A. Macchi, “Radiation reaction effects on radiation pressure acceleration,” *New J. Phys.* **12**, 123005 (2010).
- [40] M. Tamburini, F. Pegoraro, A. Di Piazza, C. H. Keitel, T. V. Liseykina, and A. Macchi, “Radiation reaction effects on electron nonlinear dynamics and ion acceleration in laser-solid interaction,” *Nucl. Instrum. Methods Phys. Res., Sect. A* **653**, 181 (2011).
- [41] A. Di Piazza, C. Müller, K. Z. Hatsagortsyan, and C. H. Keitel, “Extremely high-intensity laser interactions with fundamental quantum systems,” *Rev. Mod. Phys.* **84**, 1177–1228 (2012).
- [42] Min Chen, Alexander Pukhov, Tong-Pu Yu, and Zheng-Ming Sheng, “Radiation reaction effects on ion acceleration in laser foil interaction,” *Plasma Phys. Control. Fusion* **53**, 014004 (2010).
- [43] R. Capdessus and P. McKenna, “Influence of radiation reaction force on ultraintense laser-driven ion acceleration,” *Phys. Rev. E* **91**, 053105 (2015).
- [44] F. Wan, K. Xue, Z.-K. Dou, K. Z. Hatsagortsyan, W. Yan, D. Khikhlikha, S. V. Bulanov, G. Korn, Y.-T. Zhao, Z.-F. Xu, and J.-X. Li, “Imprint of the stochastic nature of photon emission by electrons on the proton energy spectra in the laser-plasma interaction,” *Plasma Phys. Control. Fusion* **61**, 084010 (2019).
- [45] D. Seipt, D. Del Sorbo, C. P. Ridgers, and A. G. R. Thomas, “Theory of radiative electron polarization in strong laser fields,” *Phys. Rev. A* **98**, 023417 (2018).
- [46] Markus Büscher, Anna Hützen, Liangliang Ji, and Andreas Lehrach, “Generation of polarized particle beams at relativistic laser intensities,” *High Power Laser Sci. Eng.* **8**, e36 (2020).
- [47] Kun Xue, Zhen-Ke Dou, Feng Wan, Tong-Pu Yu, Wei-Min Wang, Jie-Ru Ren, Qian Zhao, Yong-Tao Zhao, Zhong-Feng Xu, and Jian-Xing Li, “Generation of highly-polarized high-energy brilliant γ -rays via laser-plasma interaction,” *Matter Radiat. Extremes* **5**, 054402 (2020).
- [48] Yan-Fei Li, Rashid Shaisultanov, Karen Z. Hatsagortsyan, Feng Wan, Christoph H. Keitel, and Jian-Xing Li, “Ultrarelativistic electron-beam polarization in single-shot interaction with an ultraintense laser pulse,” *Phys. Rev. Lett.* **122**, 154801 (2019).
- [49] Yan-Fei Li, Rashid Shaisultanov, Yue-Yue Chen, Feng Wan, Karen Z. Hatsagortsyan, Christoph H. Keitel, and Jian-Xing Li, “Polarized ultrashort brilliant multi-GeV γ rays via single-shot laser-electron interaction,” *Phys. Rev. Lett.* **124**, 014801 (2020).
- [50] Wei-Yuan Liu, Kun Xue, Feng Wan, Min Chen, Jian-Xing Li, Feng Liu, Su-Ming Weng, Zheng-Ming Sheng, and Jie Zhang, “Trapping and acceleration of spin-polarized positrons from γ photon splitting in wakefields,” *Arxiv* (2020), arXiv:2011.00156 [physics.plasm-ph].
- [51] Ren-Tong Guo, Yu Wang, Rashid Shaisultanov, Feng Wan, Zhong-Feng Xu, Yue-Yue Chen, Karen Z. Hatsagortsyan, and Jian-Xing Li, “Stochasticity in radiative polarization of ultra-relativistic electrons in an ultrastrong laser pulse,” *Phys. Rev. Research* **2**, 033483 (2020).
- [52] T. D. Arber, K. Bennett, C. S. Brady, A. Lawrence-Douglas, M. G.

- Ramsay, N J Sircombe, P Gillies, R G Evans, H Schmitz, A R Bell, and C P Ridgers, “Contemporary particle-in-cell approach to laser-plasma modelling,” *Plasma Phys. Control. Fusion* **57**, 113001 (2015).
- [53] Andrea Macchi, Silvia Veghini, and Francesco Pegoraro, ““light sail” acceleration reexamined,” *Phys. Rev. Lett.* **103**, 085003 (2009).
- [54] B. Qiao, M. Zepf, M. Borghesi, and M. Geissler, “Stable GeV ion-beam acceleration from thin foils by circularly polarized laser pulses,” *Phys. Rev. Lett.* **102**, 145002 (2009).
- [55] B. Qiao, M. Zepf, M. Borghesi, B. Dromey, M. Geissler, A. Karmakar, and P. Gibbon, “Radiation-pressure acceleration of ion beams from nanofoil targets: The leaky light-sail regime,” *Phys. Rev. Lett.* **105**, 155002 (2010).
- [56] See supplemental materials for details on analytical expressions of relativistic ponderomotive force and relative slippage distance, electron energy spectrum, and phase space evolution of protons.
- [57] Feng Wan, Yu Wang, Ren-Tong Guo, Yue-Yue Chen, Rashid Shaisultanov, Zhong-Feng Xu, Karen Z. Hatsagortsyan, Christoph H. Keitel, and Jian-Xing Li, “High-energy γ -photon polarization in nonlinear breit-wheeler pair production and γ polarimetry,” *Phys. Rev. Research* **2**, 032049 (2020).
- [58] L. H. Thomas, “The motion of the spinning electron,” *Nature (London)* **117**, 514 (1926).
- [59] L. H. Thomas, “The kinematics of an electron with an axis,” *Philos. Mag.* **3**, 1–22 (1927).
- [60] V. Bargmann, Louis Michel, and V. L. Telegdi, “Precession of the polarization of particles moving in a homogeneous electromagnetic field,” *Phys. Rev. Lett.* **2**, 435–436 (1959).
- [61] N.S.P King, E Ables, Ken Adams, K.R Alrick, J.F Amann, Stephen Balzar, P.D Barnes Jr, M.L Crow, S.B Cushing, J.C Eddleman, T.T Fife, Paul Flores, D Fujino, R.A Gallegos, N.T Gray, E.P Hartouni, G.E Hogan, V.H Holmes, S.A Jaramillo, J.N Knudsson, R.K London, R.R Lopez, T.E McDonald, J.B McClelland, F.E Merrill, K.B Morley, C.L Morris, F.J Naivar, E.L Parker, H.S Park, P.D Pazuchanics, C Pillai, C.M Riedel, J.S Sarracino, F.E Shelley Jr, H.L Stacy, B.E Takala, Richard Thompson, H.E Tucker, G.J Yates, H.-J Ziock, and J.D Zumbro, “An 800-MeV proton radiography facility for dynamic experiments,” *Nucl. Instrum. Meth. A.* **424**, 84–91 (1999).
- [62] W. P. Wang, C. Jiang, H. Dong, X. M. Lu, J. F. Li, R. J. Xu, Y. J. Sun, L. H. Yu, Z. Guo, X. Y. Liang, Y. X. Leng, R. X. Li, and Z. Z. Xu, “Hollow plasma acceleration driven by a relativistic reflected hollow laser,” *Phys. Rev. Lett.* **125**, 034801 (2020).
- [63] Hamlet Karo Avetissian, *Relativistic nonlinear electrodynamics: interaction of charged particles with strong and super strong laser fields*, Springer series in optical sciences, (Springer, New York, 2006) pp. xiii, 333 p.
- [64] E.L. Lindman and M.A. Stroschio, “On the relativistic corrections to the ponderomotive force,” *Nucl. Fusion* **17**, 619–621 (1977).
- [65] Brice Quesnel and Patrick Mora, “Theory and simulation of the interaction of ultraintense laser pulses with electrons in vacuum,” *Phys. Rev. E* **58**, 3719–3732 (1998).
- [66] F. Niel, C. Riconda, F. Amiranoff, R. Ducloux, and M. Grech, “From quantum to classical modeling of radiation reaction: A focus on stochasticity effects,” *Phys. Rev. E* **97**, 043209 (2018).
- [67] V. N. Baier, V. M. Katkov, and V. M. Strakhovenko, *Electromagnetic Processes at High Energies in Oriented Single Crystals* (World Scientific, 1998).
- [68] Sergei V. Bulanov, Timur Zh. Esirkepov, Masaki Kando, James K. Koga, Tatsufumi Nakamura, Stepan S. Bulanov, Alexei G. Zhidkov, Yoshiaki Kato, and Georg Korn, “On extreme field limits in high power laser matter interactions: radiation dominant regimes in high intensity electromagnetic wave interaction with electrons,” in *High-Power, High-Energy, and High-Intensity Laser Technology; and Research Using Extreme Light: Entering New Frontiers with Petawatt-Class Lasers*, Vol. 8780, edited by Georg Korn, Luis Oliveira Silva, and Joachim Hein, International Society for Optics and Photonics (SPIE, 2013) pp. 185 – 199.
- [69] N. Neitz and A. Di Piazza, “Stochasticity effects in quantum radiation reaction,” *Phys. Rev. Lett.* **111**, 054802 (2013).
- [70] V. A. Vshivkov, Naumova, N. M., F. Pegoraro, and S. V. Bulanov, “Nonlinear electrodynamics of laser pulse interaction with a thin foil,” *Phys. Plasmas* **5**, 2727 (1998).
- [71] S. S. Bulanov, E. Esarey, C. B. Schroeder, S. V. Bulanov, T. Zh. Esirkepov, M. Kando, F. Pegoraro, and W. P. Leemans, “Radiation pressure acceleration: The factors limiting maximum attainable ion energy,” *Phys. Plasmas* **23**, 056703 (2016).